POST-WILDFIRE TERRAIN EVOLUTION IN AN ALPINE AREA

Monica Corti[1]

Laura Corti[1]

PhD. Andrea Abbate[2]

Prof. Monica Papini[1]

Assoc. Prof. Laura Longoni[1]

[1] Department of Civil and Environmental Engineering (DICA), Politecnico di Milano, **Italy**
[2] Ricerca sul Sistema Energetico – RSE S.p.A, Milano, **Italy**

ABSTRACT

In a climate change scenario, natural disasters as wildfires and their consequences are expected to increase. Besides the loss of vegetation, wildfires have severe effects over mountain environments, frequently affecting slope stability and eventually provoking further economic losses and casualties. The risen probability of flash flooding and debris flow is recognized to depend on a modification of the soil hydrological properties, in particular of the soil infiltration capacity, in burnt terrains. Past studies identified different trends of soil infiltration recovery after fire, depending on the site environmental characteristics and on the original soil conditions. Even though wildfires are common in the Alpine area, studies on the hydrological impact of wildfires are mainly from the US, Australia and partly from the Iberian Peninsula. This work aims to investigate the impact of a wildfire occurred in 2019 in the Southern Alps and to retrieve recovery trends for the calibration of a simple 1D hydrogeological model. The effects of the wildfire and their variations over time were evaluated on three different spatial scales: satellite imagery, field monitoring (infiltration tests) and laboratory rainfall simulations.

Keywords: wildfire, infiltration rate, single-ring infiltrometer, hydraulic conductivity, climate change

INTRODUCTION

As reported in many literatures works, wildfire events have severe impacts over mountain slope environments, not only in terms of loss of vegetation, but also regarding the terrain hydrological conditions. After wildfires, an increase of flooding and debris flows hazard in predisposed areas is indeed often observed [1, 2]. Authors found this increase to be related to a change in water circulation of the burnt site that recovers in several years [3], depending on the vegetation characteristics of the site, on the meteorological conditions after fire, and on the fire severity [4]. The most critical factors causing this higher hazard are the quicker response to precipitations that generates higher streamflow volumes and the increased erosive action of the rain splash, which are due to the reduction of the canopy interception [5]. Another relevant parameter is the modification of the natural soil water repellency, a common characteristic of soils under conifer forests, that can lead to a change in the infiltration capacity and to a further increase of runoff and erosion [2, 6].

https://doi.org/10.5593/sgem2022/3.1/s12.20

These types of forests often show a superficial wettable and erodible layer overlying a water repellent soil layer after a high-fire severity wildfire. This shallow wettable layer is less cohesive and susceptible to quick saturation, often resulting in slope instabilities [2].

This work focuses on an Alpine wildfire case study in order to derive the impact on the hydrological conditions of the slope at different scales, and to evaluate the recovery time of soils to pre-fire conditions. Soil burning conditions and their evolutions were monitored after the wildfire over the span of three years by field surveys and by remote sensing analyses.

Field surveys were distributed on three different sub-areas, two inside the wildfire area and one outside, for comparison to pre-fire conditions. Falling-head infiltration tests were performed to investigate the soil hydrological properties of the three areas over time. At the same time, Sentinel-2 images from the European Copernicus mission were implied for remote monitoring of the study area. Remote sensing allows burnt areas to be identified at larger scales throughout indices based on vegetation reflectance. Also, it enables to estimate fire severity, which is often difficult to derive because the temperatures reached are normally unknown, and to investigate large areas, with a high temporal resolution and low cost. It was found that the burnt area still presented a different response to precipitation three years after the wildfire, which implies no full recovery yet. A recovery trend was identified by the Sentinel-2 imagery analysis. The presented study aims to bring out important considerations on post-fire recovery for hydrological models.

METERIALS & METHODS

The study area is located in Sorico municipality, northern Italy, in Central Alps (Figure 1). Here, a wildfire event took place from the 30th December 2018 to the 17th January 2019, burning an approximative area of 1 km^2. The burnt area is on a watershed exposed to south at an elevation around 1000 m asl. The area presents coniferous woods in the less steep part of the slope, and grasslands and shrubs where the slope is steeper (> 25°). Geologically speaking, the area is covered by glacial deposits from the Last Glacial Maximum and by recent colluvial deposits. The regolith has a heterogeneous granulometry and has an average thickness of one meter. The outcrops consist of gneiss from the zone of Bellinzona-Dascio (BD), a high-grade metamorphic unit, composed by different types of gneisses, minor marble lenses, amphibolites and ophiolitic rocks.

Monitoring was distributed over two different vegetation sub-areas inside the former wildfire perimeter, one characterized by burnt conifer woods and the other by grassland. The third monitored sub-area was in a conifer woods, located outside the burnt area, and it was taken into account for comparison.

The remote sensing analysis was performed through different remote sensing indices, computed from Copernicus Sentinel-2 raw bands (complete list in Table 1). These indices mainly consider spectral bands that refer to living vegetation characteristics, as Red wavelengths, where there are chlorophyll absorption peaks, and Near InfraRed, where the high reflectance of vegetation itself is located, which represents the integrity of leaf cell structure, or as Short-Wave InfraRed, where there are the water absorption peaks, which can be used to detect the decrease of leaves water content related to the burning of vegetation. In particular, the NIR band and the SWIR bands result to be the most sensitive for wildfire detection, as they experience the largest changes comparing pre-fire and

post-fire conditions [7, 8]. Specific indicators of fire occurrence were also considered, as the Normalized Burn Ratio (NBR) and as the Burned Area Index (BAI), which is related to charcoal presence on the ground.

Fire severity and its change over time was also estimated, considering the difference of NDVI and NBR indices before and after fire, following [9] classification. Initial fire severity is shown in Figure 1.

Sentinel-2 images were selected considering favourable meteorological conditions, with a maximum cloud coverage of 30%, and without snow cover, in order to avoid alterations in the moisture evaluations.

Table 1. Remote sensing indices taken into account for the burnt recovery analysis, referred to Sentinel-2 spectral bands (B3 is Green, B4 is Red, B8 is Near InfraRed, B8A is Narrow NIR, B11 and B12 are Short-Wave InfraRed).

Index	Equation
False Color	$[B8 \mid B4 \mid B3]$
Normalized Difference Vegetation Index (NDVI)	$\frac{B8 - B4}{B8 + B4}$
Moisture Index (MI)	$\frac{B8A - B11}{B8A + B11}$
Moisture Index (MSI)	$\frac{B11}{B8}$
Normalized Difference Moisture Index (NDMI)	$\frac{B8 - B11}{B8 + B11}$
Normalized Difference Water Index (NDWI)	$\frac{B3 - B8}{B3 + B8}$
Normalized Burn Ratio (NBR)	$\frac{B8 - B12}{B8 + B12}$
Burned Area Index (BAI)	$\frac{1}{(0.1 - B4)^2 + (0.06 - B8)^2}$

Falling-head infiltration tests were performed to assess post-fire infiltration capacity of soils in the three sub-areas, and their potential change over time. The tests were carried out using a single-ring infiltrometer and a double-ring infiltrometer. The single-ring infiltrometer was a plastic tube with a diameter of 12 cm and a height of 100 cm. The double-ring apparatus was composed by two stainless steel cylinders with a height of 15 cm and diameters of 30 and 60 cm. The main advantage of this kind of test is the low cost, particularly for the plastic single-ring infiltrometer. Falling-head method was preferred to the constant-head method because of the lack of water supply in the nearby of the study area, given that falling-head tests require less water. The test procedure consisted in pouring water into the infiltrometer, and then measuring the variation of the hydraulic head over time. The obtained infiltration rate was corrected to exclude lateral flow divergence component by single-ring tests results, measuring the distance of lateral wetting as in [10]. The resulting data of infiltration velocity versus test time are infiltration curves that follow the exponential model from Horton [11]:

$$f = f_C + (f_0 - f_C)e^{-K_f t} \quad \text{(Eq. 1)}$$

https://doi.org/10.5593/sgem2022/3.1/s12.20

were f_c is the field capacity, the asymptotic value of infiltration rate that is related to saturated hydraulic conductivity, f_0 is the initial infiltration rate, which is inversely proportional to the initial soil moisture, and K is a decay constant.

The obtained field infiltration rates were fitted to the following simpler exponential equation, where "a" is the difference between f_0 and f_c, and "b" corresponds to the decay constant K of Horton's model:

$$V_{inf} = ae^{-bt} \quad \text{(Eq. 2).}$$

These fitting coefficients, a and b, and an approximated f_c value, considered as the infiltration rate value at 4000 s, were evaluated for the three zones over time.

Hydraulic conductivity was also estimated as in the Lefranc infiltration test procedure [12]. Moreover, during the first survey (October 2019), burnt and unburnt soil samples were collected to evaluate their saturated hydraulic conductivity in laboratory, using a falling-head permeameter [13].

Relations between all the parameters measured on the field over time (a, b, f_c, k) and some meteorological variables (cumulative rainfall of the ten and twenty days prior the survey, solar radiation, temperature and relative humidity) were also investigated by factor analysis (principal components analysis method) [14].

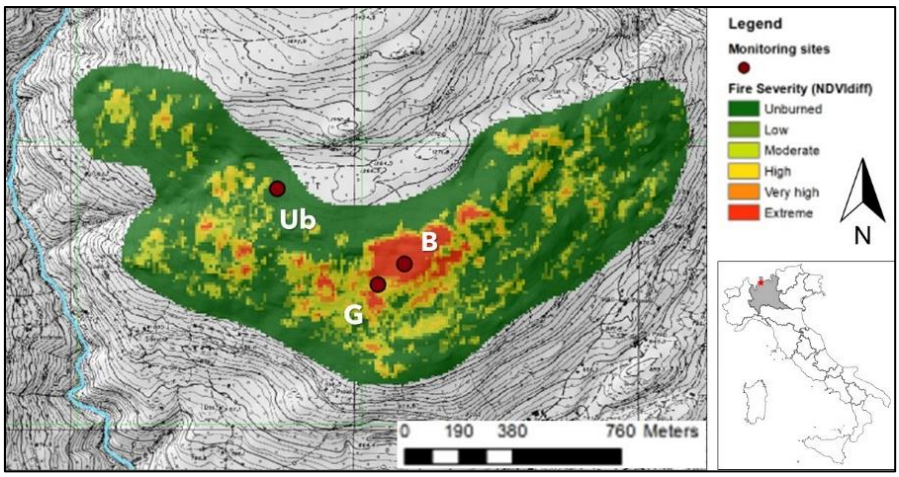

Figure 1. Location of the study area and of the three sub-areas identified for monitoring (B is burnt woods, G is burnt grassland, Ub is unburned woods). Fire severity is also displayed as the difference of NDVI before and after the wildfire, according to [9].

RESULTS AND DISCUSSION

The post-fire field monitoring started in October 2019, ten months after the wildfire event. Over the span of three years, a first vegetation recovery was observed in the burnt woods area, which was initially characterized by almost bare soil and by some burnt pine trees. In May 2022, even if all the burnt plants were still in place, the same area showed grass and pioneer vegetation. On the other hand, the "grassland" sub-area presented already grass in October 2019, even if fire prints were still recognisable in the burnt shrubs. In general, all the infiltration parameters evaluated on the field appear to be almost constant

over time both for the burnt woods and for the grassland. Boxplots of the parameters of the whole burnt area are reported in Figure 2. The median values of K and f_c appears to be similar to the K_s of the unburned soil, gained from the permeability test in laboratory.

This indicates that hydraulic conductivity of soils was already similar in the three zones ten months after the wildfire. On the other hand, differences among the three areas are still present, if we consider the shape of the infiltration curves. In particular, a e b coefficients were more variable in the unburned woods than in the formerly burnt area, as visible from the bar plots in Figure 3. The factor analysis (Table 2) shows a weak correlation between f_c and some meteorological parameters, as temperature and rainfall for the burnt woods, a correlation between K and all the meteorological parameters in the formerly burnt grassland, and no correlations in the unburned woods. The formerly burnt grassland shows also an evolution of a and b over time, where a increases and b decreases (Figure 2c and Figure 2d).

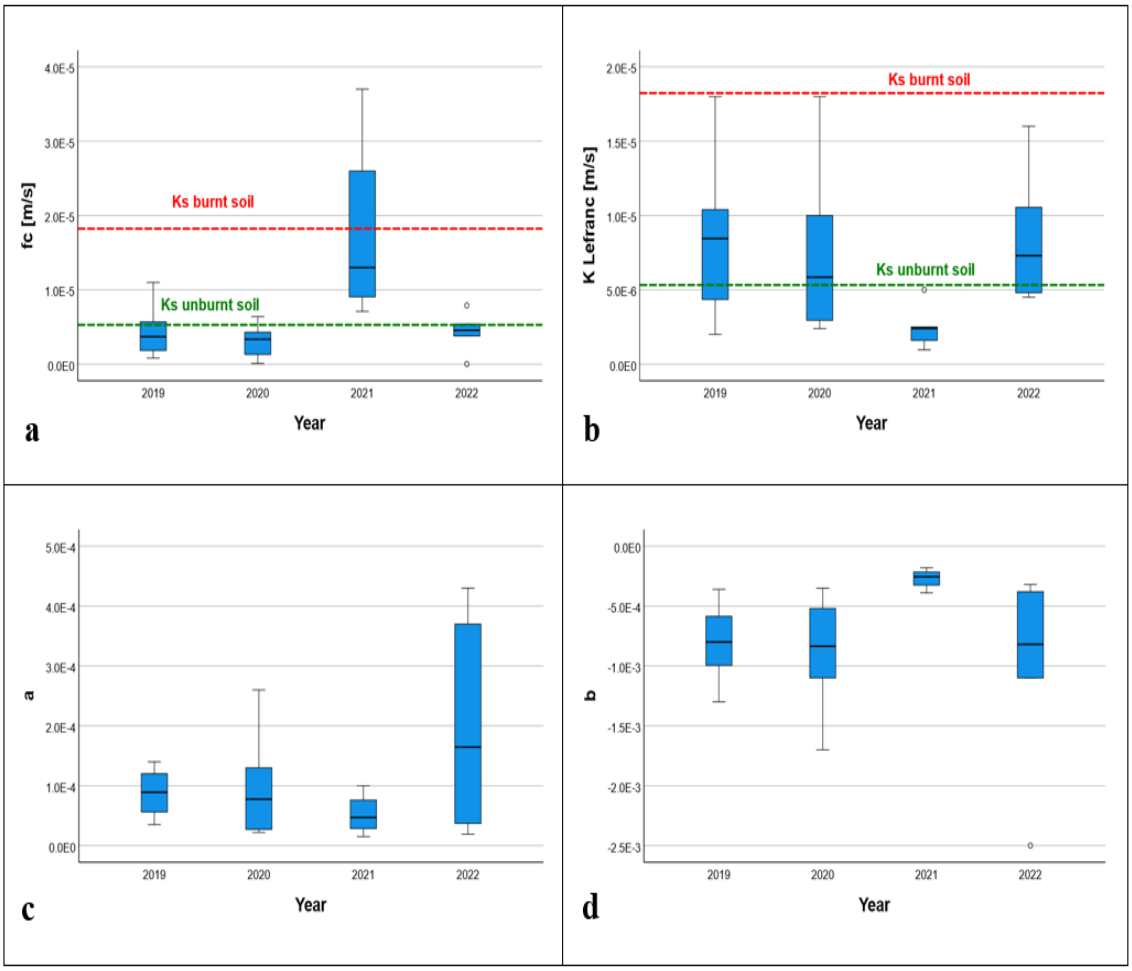

Figure 2 Boxplots of the infiltration parameters measured on the field inside the burnt area (burnt woods and burnt grassland); a) field capacity (fc) estimated from Horton curves fitting, b) hydraulic conductivity (K) estimated with Lefranc method, c) a fitting coefficient of exponential infiltration rate curves, d) b fitting coefficient of exponential infiltration rate curves. In a) and b), f_c and K are compared to the K_s of burnt and unburned soils measured by falling-head permeameter in laboratory.

https://doi.org/10.5593/sgem2022/3.1/s12.20

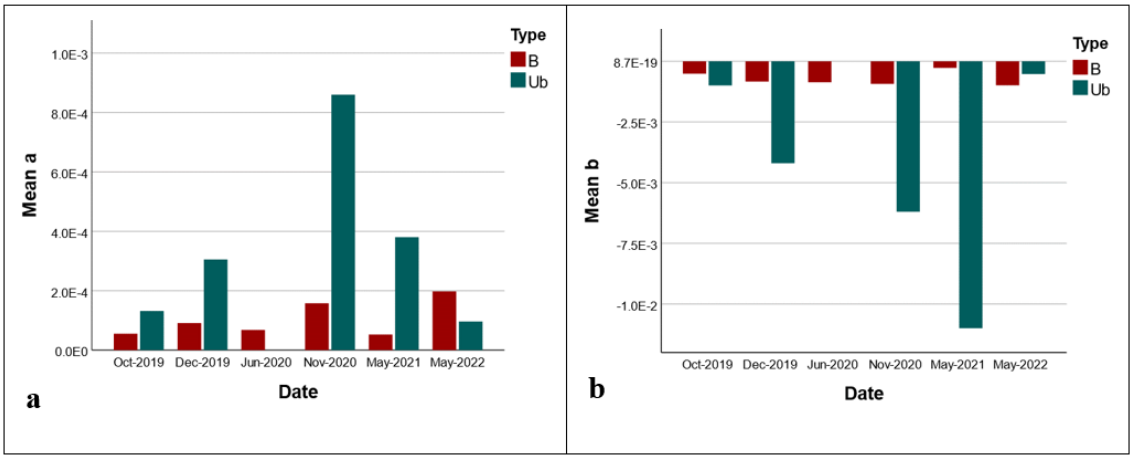

Figure 3 Bar plots of a and b after falling-head infiltration tests performed in the burnt area (burnt woods and burnt grassland) and in the unburned woods.

These variations in the correlation matrices were interpreted as dependent on the remaining difference of the coverage conditions among the three areas, as the conifers seem to protect soils from the meteorological variables. This effect is bigger in the unburned area, but it is also partly present inside the formerly burnt woods, where many burnt trees still stand three years after the fire.

Table 2 Factor analysis correlation matrix.

		K [m/s]	fc [m/s]	a	b	rain mm/10day	rain mm/20day	rad	temp	humidity	days after fire
Burnt woods	**K [m/s]**	1.00	-0.48	0.81	-0.74	-0.15	-0.27	0.10	0.17	0.13	0.06
	fc [m/s]	-0.48	1.00	-0.37	0.79	0.16	0.38	-0.17	-0.34	0.01	0.19
	a	0.81	-0.37	1.00	-0.61	-0.11	-0.12	-0.01	0.03	0.15	0.26
	b	-0.74	0.79	-0.61	1.00	0.10	0.28	-0.14	-0.25	0.01	0.18
	rain mm/10day	-0.15	0.16	-0.11	0.10	1.00	0.92	-0.93	-0.90	0.73	-0.56
	rain mm/20day	-0.27	0.38	-0.12	0.28	0.92	1.00	-0.86	-0.91	0.60	-0.29
	rad	0.10	-0.17	-0.01	-0.14	-0.93	-0.86	1.00	0.97	-0.88	0.37
	temp	0.17	-0.34	0.03	-0.25	-0.90	-0.91	0.97	1.00	-0.83	0.24
	humidity	0.13	0.01	0.15	0.01	0.73	0.60	-0.88	-0.83	1.00	-0.16
	days after fire	0.06	0.19	0.26	0.18	-0.56	-0.29	0.37	0.24	-0.16	1.00
Burnt grassland	**K [m/s]**	1.00	-0.40	0.33	-0.30	0.45	0.44	-0.50	-0.39	0.30	-0.20
	fc [m/s]	-0.40	1.00	-0.22	0.53	-0.15	0.13	0.24	0.04	-0.40	0.28
	a	0.33	-0.22	1.00	-0.93	-0.17	-0.02	-0.06	-0.08	0.11	0.76
	b	-0.30	0.53	-0.93	1.00	0.08	0.05	0.16	0.12	-0.29	-0.57
	rain mm/10day	0.45	-0.15	-0.17	0.08	1.00	0.93	-0.97	-0.95	0.85	-0.63
	rain mm/20day	0.44	0.13	-0.02	0.05	0.93	1.00	-0.92	-0.96	0.72	-0.39
	rad	-0.50	0.24	-0.06	0.16	-0.97	-0.92	1.00	0.98	-0.92	0.48
	temp	-0.39	0.04	-0.08	0.12	-0.95	-0.96	0.98	1.00	-0.88	0.37
	humidity	0.30	-0.40	0.11	-0.29	0.85	0.72	-0.92	-0.88	1.00	-0.42
	days after fire	-0.20	0.28	0.76	-0.57	-0.63	-0.39	0.48	0.37	-0.42	1.00
Unburned woods	**K [m/s]**	1.00	-0.50	0.36	-0.72	-0.03	-0.07	-0.01	-0.04	-0.03	-0.17
	fc [m/s]	-0.50	1.00	-0.43	0.50	-0.12	0.05	0.05	-0.09	-0.03	0.49
	a	0.36	-0.43	1.00	-0.71	0.23	0.29	-0.18	-0.09	0.04	0.08
	b	-0.72	0.50	-0.71	1.00	-0.17	-0.26	0.07	0.06	0.00	-0.10
	rain mm/10day	-0.03	-0.12	0.23	-0.17	1.00	0.92	-0.76	-0.59	0.86	-0.23
	rain mm/20day	-0.07	0.05	0.29	-0.26	0.92	1.00	-0.65	-0.57	0.66	0.10
	rad	-0.01	0.05	-0.18	0.07	-0.76	-0.65	1.00	0.93	-0.69	0.43
	temp	-0.04	-0.09	-0.09	0.06	-0.59	-0.57	0.93	1.00	-0.48	0.32
	humidity	-0.03	-0.03	0.04	0.00	0.86	0.66	-0.69	-0.48	1.00	-0.28
	days after fire	-0.17	0.49	0.08	-0.10	-0.23	0.10	0.43	0.32	-0.28	1.00

The analysis by remote sensing suggests a complete recovery of the site in almost seven years after the wildfire event (Figure 4), following a logarithmic recovery trend as in [15].

This recovery is here intended as a sort of full recovery of the canopy protection, as satellites are not able to derive hydrological characteristics of soils if burnt trees, identified as dark pixels, are still in place.

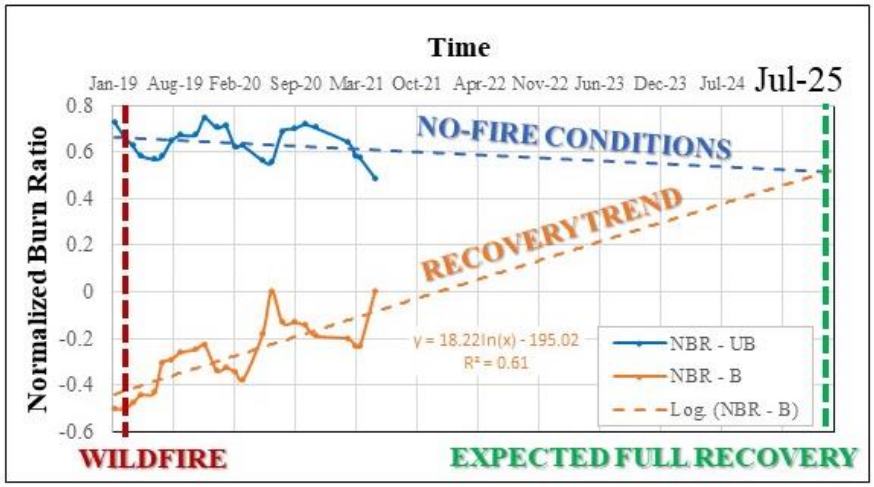

Figure 4 Recovery trend derived by remote sensing analysis. The orange line is referred to as to the burnt woods (B) and the blue line is referred to the unburned woods (Ub).

CONCLUSION

A burnt area in the Alps was monitored over the span of three years by field falling-head infiltration tests and by remote sensing. Despite an initial recovery of vegetation is recognised, wildfire effects remain four years after the event. In particular, the coefficients of the exponential infiltration curves have a different behaviour over time in the burnt area from the unburnt area. Even if the estimated field capacity (f_c) and the hydraulic conductivity of burnt soils always have similar values to the saturated hydraulic conductivity of unburnt soils estimated in laboratory, they appear to be correlated with the meteorological variables, whereas in the unburned zone it does not occur. This characteristic was interpreted as a direct response to precipitation due to the absence of a complete restored vegetation coverage. Falling-head tests did not suggest a recovery time for the whole burnt area, even if exponential coefficients of the grassland sun-area are correlated with time.

Anyway, a logarithmic recovery trend was derived from the NBR evolution over time, which indicates full recovery of the site in almost seven years after the wildfire event. This recovery is intended as a recovery of the canopy protection, an important parameter for soil protection from erosion.

REFERENCES

[1] Abbate, A., Longoni, L., Ivanov, V. I., & Papini, M., Wildfire impacts on slope stability triggering in mountain areas, Geosciences, Switzerland, vol. 9/issue 10, pp 417, 2019;

[2] Doerr, S. H., Shakesby, R. A., Blake, W. H., Chafer, C. J., Humphreys, G. S., & Wallbrink, P. J., Effects of differing wildfire severities on soil wettability and

https://doi.org/10.5593/sgem2022/3.1/s12.20

implications for hydrological response, Journal of Hydrology, vol. 319/issue 1–4, pp 295–311, 2006;

[3] Larson-Nash, S. S., Robichaud, P. R., Pierson, F. B., Moffet, C. A., Williams, C. J., Spaeth, K. E., Brown, R. E., & Lewis, S. A., Recovery of small-scale infiltration and erosion after wildfires, Journal of Hydrology and Hydromechanics, vol. 66/issue 3, pp 261–270, 2018;

[4] Rodríguez-Alleres, M., Varela, M. E., & Benito, E., Natural severity of water repellency in pine forest soils from NW Spain and influence of wildfire severity on its persistence, Geoderma, vol. 191, pp 125–131, 2012;

[5] Stoof, C. R., Vervoort, R. W., Iwema, J., VanDenElsen, E., Ferreira, A. J. D., & Ritsema, C. J., Hydrological response of a small catchment burned by experimental fire, Hydrology and Earth System Sciences, vol. 16/issue 2, pp 267–285, 2012;

[6] Butzen, V., Seeger, M., Marruedo, A., de Jonge, L., Wengel, R., Ries, J. B., & Casper, M. C., Water repellency under coniferous and deciduous forest - Experimental assessment and impact on overland flow, Catena, vol. 133, pp 255–265, 2015;

[7] Gao, B.-C., NDWI—A normalized difference water index for remote sensing of vegetation liquid water from space, Remote Sensing of Environment, vol. 58/issue 3, pp 257–266, 1996;

[8] Han, A., Qing, S., Bao, Y., Na, L., Bao, Y., Liu, X., Zhang, J., & Wang, C., Short-term effects of fire severity on vegetation based on sentinel-2 satellite data, Sustainability, Switzerland, vol. 13/issue 1, pp 1–22, 2021;

[9] Chafer, C. J., Noonan, M., & Macnaught, E., The post-fire measurement of fire severity and intensity in the Christmas 2001 Sydney wildfires, International Journal of Wildland Fire, vol. 13/issue 2, pp 227–240, 2004;

[10] Bouwer, H., Back, J. T., & Oliver, J. M., Predicting infiltration and ground-water mounds for artificial recharge, Journal of Hydrologic Engineering, vol. 4/issue 4, pp 350–357, 1999;

[11] Horton, R. E., An approach toward a physical interpretation of infiltration-capacity, Soil Science Society of America Journal, vol. 5/issue C, pp 399–417, 1941;

[12] Association Française de Normalisation (AFNOR), Reconnaissance et essais, Essai d'eau LEFRANC [Recognition and tests, LEFRANC water test], Norme Française NF P 94-132 Sols, 2000 (in French);

[13] Olson, R. E., & Daniel, D. E., Measurement of the Hydraulic Conductivity of Fine-Grained Soils, ASTM Special Technical Publication, pp 18–64, 1981;

[14] Bro, R., & Smilde, A. K., Principal component analysis, Analytical methods, vol. 6/issue 9, pp 2812-2831, 2014;

[15] Ryu, J. H., Han, K. S., Hong, S., Park, N.-W., Lee, Y.-W., Cho, J., Satellite-Based Evaluation of the Post-Fire Recovery Process from the Worst Forest Fire Case in South Korea, Remote Sensing, vol. 10/issue 6, pp 918, 2018.